Parkinson's protein α-synuclein : membrane interactions and fibril structure

Kumar, P.

1 Introduction

Parkinson's disease (PD) (1) is the second most highly spread neurodegenerative disease after Alzheimer's (2), and affects primarily the elderly population (2,3). The clinical effect of PD is associated with the loss of dopaminergic neurons from part of the mid-brain called *substantia nigra pars compacta* (2,4,5). The most common symptoms of PD are movement-related such as resting tremor, bradykinesia, muscular rigidity and postural instability (2,4,5). These symptoms were first described by James Parkinson in 1817 (1). Moreover, patients may have other problems like depression, olfactory deficits, psychosis, cognitive impairment and sleeping problems (6–8). To find a cure to PD is still difficult, because the symptoms of the disease are not early detectable. PD is characterized by the presence of Lewy bodies in the patient's brain (9). The Lewy body is a protein deposit, which mainly consists of aggregates of α-Synuclein (9,10). This protein is expressed abundantly in the brain and localizes in the presynaptic terminal of nerve cells (11,12).

This thesis focuses on the protein α-Synuclein (αS). Its ability to interact with membranes as well as to form amyloid fibrils in certain conditions are the main aspects of this thesis. Spin-label electron paramagnetic resonance (EPR) is the method used to study these complex processes. This chapter presents a brief introduction to this thesis. We describe the protein αS, its membrane interaction, fibrils, and spin-label EPR.

1.1 α-Synuclein and its properties

The protein αS consists of 140 amino acids. It lacks a defined secondary structure in solution at neutral pH (13,14) and is a member of the intrinsically disordered protein (IDP) class (15,16). The amino acid sequence of αS can be divided into two major regions: a) the N-terminal region (residues 1-100), which can be further

divided into two sub regions: a highly positively charged region (residues from 1-60), and a hydrophobic non-amyloid-beta-component (NAC) region (residues 61-94); and b) the C-terminal region (residues 100-140), which is rich in negatively charged amino acids, especially glutamate (see Figure 1.1).

The N-terminal region contains the seven imperfect repeats (KTKEGV consensus sequence) spread from residue 7 to residue 87 (11,17), and has a tendency to form an α-helical conformation upon membrane binding (14,18–21). The three most common point mutations in αS linked to PD are A30P (22), E46K (23), A53T (24). In addition, two other point mutations G51D (25), H50Q (26), and A53E (92) have been described recently. They are all located in the N-terminal region of αS. The NAC region plays a crucial role in the aggregation of αS (27), and the C-terminal part of αS remains largely unstructured under most conditions (18).

Like other proteins, αS can undergo posttranslational modification (PTM). Phosphorylation (28–30), ubiquitination (31) , oxidation (32), and truncation (33) are commonly found PTMs in αS. These PTMs have an impact on the structure and function of αS (34,35).

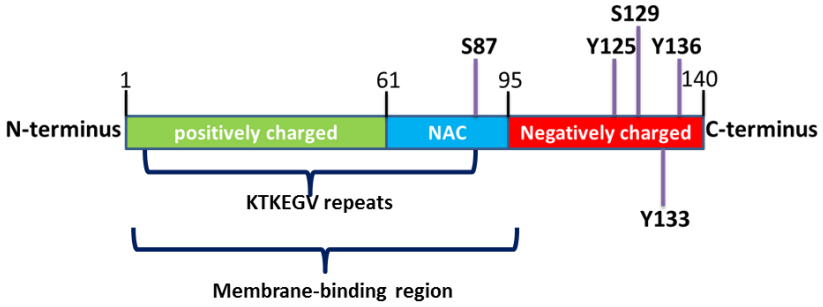

Figure 1.1. Schematic representation of the αS sequence and its different regions: The N-terminal region contains the highly positively charged region (in green), the KTKEGV repeats, and the central region (in blue), also called the NAC region. The C-terminal region (in red), the negatively charged region, contains most of the phosphorylation sites. The NAC region also contains a phosphorylation site at serine (S) 87. The numbers mark the residues and the numbers in bold the phosphorylation sites of αS.

1.2 α-Synuclein and membrane interaction

One of the proposed physiological functions of αS is neurotransmitter release (Figure 1.2) (36). In this process, αS is believed to interact with synaptic vesicles, to cluster them and bring them in close proximity of the presynaptic membrane. The protein αS also interacts with SNARE complex proteins (37,38) at synaptic vesicles. Besides in presynaptic terminals, αS is also found in the mitochondria. The presence of αS in mitochondria disturbs the functioning of mitochondria (mitochondrial dysfunction) (39–41). These functions involve the interaction of αS with membranes.

In vitro studies suggest that early-onset PD mutations do not only affect the aggregation tendency of αS, but also modulate the αS-membrane interaction (19,21,42). These observations make the interaction of αS with membranes of great interest. Therefore, the αS-membrane interaction was studied (43–64), mostly using membranes composed of simple lipids or binary lipid mixtures. The lipid composition of natural membranes is complicated as these natural membranes contain a complex mixture of lipids. In chapter 2 of this thesis, we investigate the interaction of αS with two natural membrane mimics, the Inner Mitochondrial membrane (IMM) and the Neuronal Plasma membrane (NPM).

The protein αS interacts with the membrane by the N-terminal part (residues 1-100) of the protein. Upon binding to membranes, αS attains an amphipathic α-helical conformation (14,18,63). The membrane-bound-N-terminal-α-helical region consists of three regions, one is called helix 1 (residues 3-37), the second is helix 2 (residues 45-92) and the third is the linker part in between the two helices (43,44). The affinity of αS to membranes depends on the negative charge density (ρ) of the membrane (54,55,63), where ρ represents the molar fraction of anionic lipids present in the membrane (56).

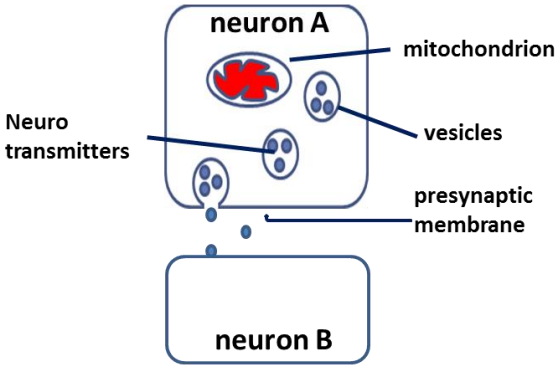

Figure 1.2. The proposed physiological function of αS: Schematic representation of a synapse showing the process of neurotransmission from neuron A to neuron B. In this process, αS interacts with vesicles loaded with neurotransmitters, clusters them and brings them to the presynaptic membrane. Vesicles fuse and release the neurotransmitters. The protein αS is present in mitochondria (shown in red) of cells, where αS interacts with the mitochondrial membranes.

If the membrane has a higher charge density (ρ = 0.5 to 1), αS binds with both helices to the membrane (Figure 1.3a). At low surface charge density (ρ < 0.5), helix 1 of αS remains attached to the membrane while helix 2 shows weak binding and detaches, starting from the C-terminal side of the protein (Figure 1.3b) (56). In connection to these observations, in chapter 2, we investigate the binding of αS with the IMM and the NPM, which have a low negative charge density of ρ = 0.2 and 0.3, respectively.

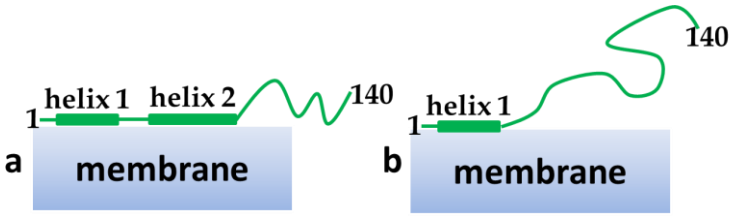

Figure 1.3. Schematic representation of αS-membrane interaction. Two conditions are shown: a. both helices of αS are completely bound to the membrane with high charge density; b. Helix 2 is detached from the membrane with low charge density, whereas αS remains bound via helix 1.

As a consequence of binding to membranes, the αS attains different conformations. On membranes, αS can be in the extended or the horseshoe conformation shown in Figure 1.4. Figure 1.4a depicts the extended conformation, and Figure 1.4b represents the horseshoe, also called the broken helix conformation. The helical region of αS has a break in the middle (residue 42 to 44), hence named linker region. The first report of the horseshoe conformation came from a solution-NMR study (43) of αS on micelles by Ulmer *et al*. (43). Later, one EPR study by Georgieva *et al*.(46) reported the presence of the extended conformation on vesicles, bicelles, and rod-like micelles, while other EPR studies (52,64) show the presence of the horseshoe conformation on vesicles and micelles.

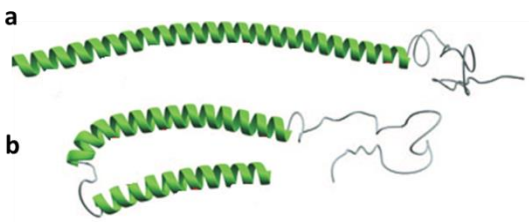

Figure 1.4. Schematic diagram of αS conformation (58) upon membrane binding: a. the extended conformation, b. the broken helix conformation also termed horseshoe conformation.

Other studies (45,51,58) found that αS coexists in both forms, the extended and the horseshoe. It is still a question whether the membrane-bound part of αS has the extended or the horseshoe form, especially when considering membranes with compositions close to natural membranes. In chapter 2 of this thesis, we report the arrangement of αS on the natural membranes IMM and NPM.

1.3 Posttranslational modification of α-Synuclein

As we mentioned above, the protein αS undergoes several modifications. The most observed and studied modification is phosphorylation, a chemical process in which a phosphate group is attached to a hydroxyl group (R-OH) (Figure 1.5). For proteins, an amino-acid residue with a hydroxyl group (for example serine (S), tyrosine (Y), and threonine (T)) is phosphorylated by enzymes, normally protein kinases, by the addition of a covalently bound phosphate group. Serine and tyrosine are the residues that undergo phosphorylation in αS. Figure 1.5 shows the phosphorylated form of serine and of tyrosine. The common phosphorylation sites of αS are shown in Figure 1.1.

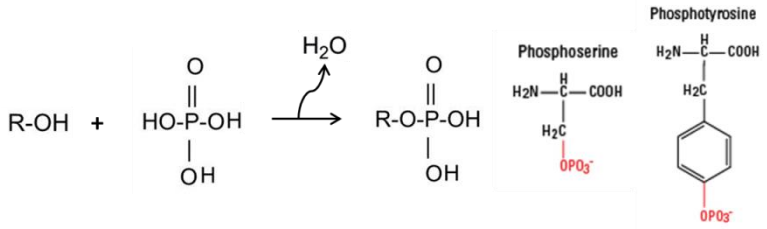

Figure 1.5. Schematic showing the process of phosphorylation and the two amino acids (serine and tyrosine) after phosphorylation: phosphoserine and phosphotyrosine.

In the Lewy bodies, αS has been found phosphorylated at residue S129 (28,65,66). The other residue found phosphorylated, albeit less than S129, is S87 (30,67). Residue S129 resides in the C-terminal part, which is not in the core of the αS fibrils (discussed below) that make up the Lewy bodies. Therefore, S129 could be more accessible to phosphorylation in the fibril/Lewy body than S87. Studies to understand the effect of phosphorylation on the aggregation and membrane binding properties of αS show conflicting results. In connection to this, we choose to investigate the relation between αS-membrane binding and phosphorylation. In chapter 3, we report how the phosphorylation of αS affects membrane binding.

1.4 α-Synuclein and fibrils

The protein αS is found as fibrillar aggregates in the Lewy bodies (9,68) where it adopts a highly ordered structure, the amyloid fibril. The amyloid fibrils have a width of approximately 10 nm and a length of a few micrometers (69). The amyloid fibril has a cross β-sheet structure (70). In these fibrils, schematically represented in Figure 1.6, individual proteins form β-strands (shown with black arrow), which arrange perpendicular to the fibril axis into a β-sheet structure (shown as grey sheets). The β-sheets grow along the fibril axis to make the protofibrils.

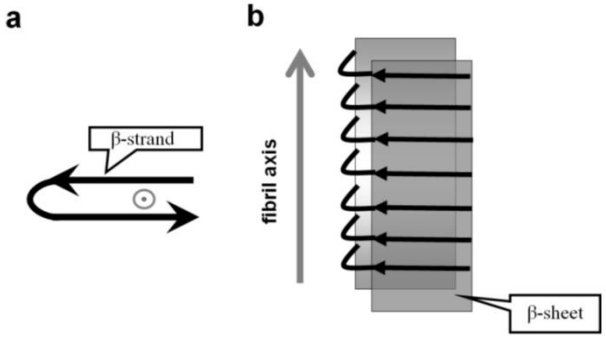

Figure 1.6. Schematic representation of amyloid fibrils . a: the black arrow shows a β-strand and the grey dot shows the direction of the fibril axis, which is pointing out of the page. b: the grey arrow shows the direction of the fibril axis. The grey planes are representative of β-sheets, which are parallel to the fibril axis. Adapted from (78).

The cross β-sheet structure is a common feature of amyloid fibrils, and many proteins are able to form fibrils. Amyloid fibrils made from the same protein can have different morphologies, a phenomenon called polymorphism. This also applies to αS fibrils. In Figure 1.7, we show transmission electron microscope (TEM) images of αS fibrils with two forms, cylindrical and twisted. The cylindrical fibrils have a uniform width indicated by black arrows in Figure 1.7a, while twisted fibrils are characterized by the twists indicated by white arrows in Figure 1.7b.

Polymorphism among fibrils can be due to a) a difference in the number of protofibrils making the fibrils (71,72), b) a different protofibrils arrangement inside fibrils, or c) a difference in the intrinsic protofibrils structure (73–75). This means that polymorphism can affect the internal fold of αS in fibrils. Since we study the fold of αS in fibrils by EPR spectroscopy in chapter 5 of this thesis, it is desired to have fibrils of similar morphology. Chapter 4 describes the TEM characterization of fibrils.

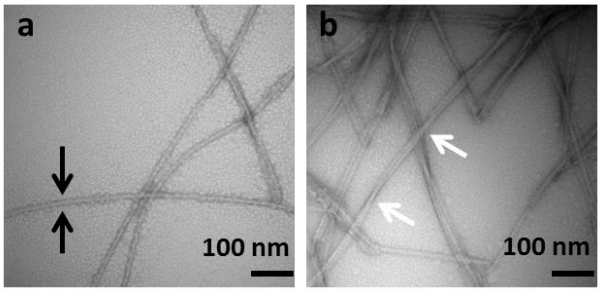

Figure 1.7. Structural characterization of two different polymorphs of αS fibrils. TEM images of αS showing a. cylindrical fibrils with uniform width, indicated by black arrows; b. twisted fibrils, where white arrows depict the points of cross-over of a twist in the fibril and the distance between the two points is called the periodicity.

1.5 Protein mediated membrane fusion

Membrane fusion is an important process in all living organisms. It is widely accepted that membrane fusion takes place in three steps, schematically represented in Figure 1.8: 1. two unfused vesicles are brought into close proximity; 2. local disruption of the outer membranes at the site of contact, also called hemifusion; 3. fusion facilitating mixing of content between the two fused vesicles (76,77). Despite this common understanding, the detailed mechanism is still lacking.

One of the best studied membrane fusion systems is the SNARE system (SNARE: soluble NSF attachment protein receptor; NSF=*N*-ethylmaleimide-sensitive factor), which involves the coiled-coil interaction between three complementary SNARE proteins (76,79). SNARE proteins are located on unfused vesicles and, in the first step of the fusion process, bind to form a tetrameric coiled-coil bringing the unfused vesicles into close contact and triggering the fusion cascade (80). In connection to that, in chapter 6 of this thesis, we investigate the first step of the fusion process, which is to bring two membranes close by the coiled-coil interaction. We use two synthetic small peptides E and K, which form K:E heterodimers with a coiled-coil structure (81). We describe in detail how the two peptides interact and arrange themselves in the coiled-coil structure.

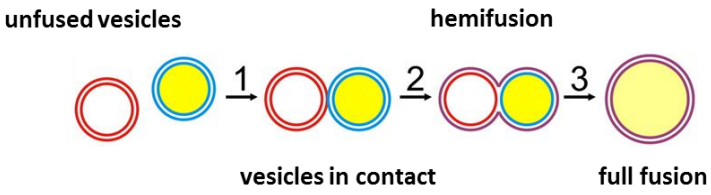

Figure 1.8. Membrane fusion steps shown with vesicles: Two unfused vesicles get closer, docking (1), mixing of outer lipid layer (hemifusion) (2) and then full fusion by mixing inner lipid layer and content (3). The Figure is modified from (77).

1.6 Spin-label EPR spectroscopy

Electron-paramagnetic-resonance (EPR) spectroscopy is a method that is sensitive to paramagnetic systems. In nature most bio-macromolecules do not contain a paramagnetic center, which makes them EPR silent. To make these molecules detectable by EPR, they need to be spin labelled. With the development of site directed spin-labelling strategies (82–84), EPR has become a powerful tool to investigate structural aspects of bio-macromolecular complexes.

Nitroxide radicals are used as spin-labels in EPR studies. The commonly used nitroxide radical is MTS ((1-oxyl-2,2,5,5-tetramethylpyrolline-3-methyl) methanethiosulfonate). Figure 1.9 shows the chemical structure of MTS. The MTS chemical structure contains a five-membered pyrroline ring with N-O bond and a methanethiosulfonate group. The unpaired electron localizes in the N-O bond shown with a black dot in Figure 1.9. The spin label attaches to a protein by a covalent bond between the –SH group of cysteine and the methanethiosulfonate of MTS.

Spin-label EPR is useful to obtain information such as: a. mobility of the spin label, b. distance between two spins, c. solvent accessibility of the spin-labelled protein site, d. polarity of the local environment of the spin label. In our research, we focus on the first two aspects. Therefore, in the following part of this chapter, we will describe briefly the effect of spin-label mobility on EPR spectra and the determination by EPR of the distance between two spins.

1.6.1 Spin-label mobility

The EPR spectrum of nitroxides is sensitive to the rotation of the spin label with respect to the external magnetic field. If the nitroxide spin label is freely mobile in solution, it exhibits an EPR spectrum with three narrow lines as shown in Figure 1.10a. The lines are spaced by the isotropic nitrogen hyperfine interaction A_{iso}, which is due to the hyperfine interaction of the unpaired electron spin S = 1/2 with the ^{14}N nuclear spin I = 1.

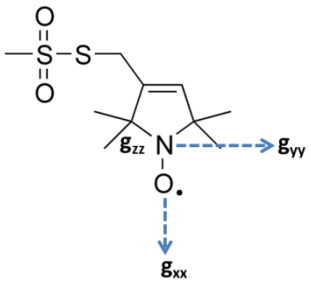

Figure 1.9. The chemical structure of the MTS nitroxide radical. The unpaired electron (shown as a black dot) localizes on the N-O bond attached to the five-membered pyrrolline ring. Principal directions of the g-tensor (blue dotted arrows) are shown. The g-tensor along the Z-direction, i.e., g_{zz} is perpendicular to the ring.

Figure 1.10 shows the effect of the spin-label mobility in terms of the rotation-correlation time (τ_r) on the line shape of the EPR spectrum by a set of simulations. At τ_r values from 0.01 ns to 0.1 ns, the line position stays fixed, and the linewidth increases in a characteristic way (Figure 1.10a and b). The line at high field broadens and shifts slightly as the rotation-correlation time increases from 0.1 ns to 1 ns. For the spectra with τ_r values of 3.2 ns and 10 ns, the line positions change and the lines at low field and high field broaden. For longer times (τ_r > 10 ns), the spectrum approaches that of a completely immobilized spin label (Figure 1.10f). In chapters 2 and 3 of this thesis, we have used the spin-label mobility to investigate the interaction of αS with membranes.

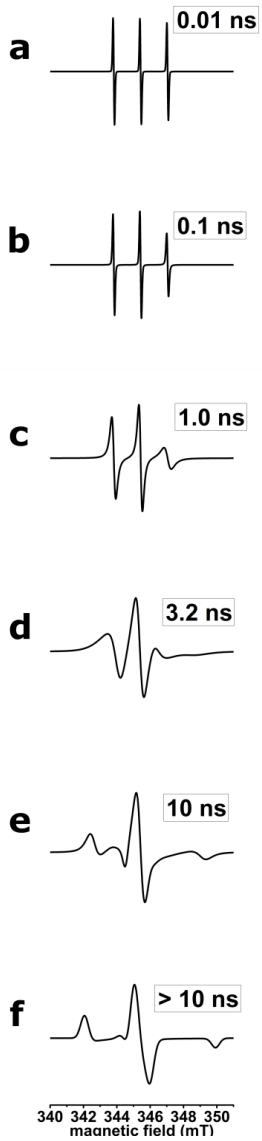

Figure 1.10. Simulated cw-EPR spectra to show the effect of the rotational motion of a nitroxide spin label on the line shape of the spectrum at room temperature. In the fast-motion regime, the three lines have almost equal intensities; a. τ_r = 0.01 ns, b. τ_r = 0.1 ns, c. τ_r = 1.0 ns, d. τ_r = 3.2 ns, e. τ_r = 10.0 ns, and f. τ_r > 10.0 ns. Spectra a to c were simulated with the algorithm "garlic", d to e with "chili" and f with "pepper" using the EasySpin (85) package. We used a g tensor [g_{xx} g_{yy} g_{zz}] = [2.009006 2.00687 2.003], and a hyperfine coupling [A_{xx} A_{yy} A_{zz}] = [13 13 110] MHz. The linewidth parameter used for spectra a to e was 0.1 mT, and for spectrum f, 0.55 mT was used.

1.6.2 Distance determination by EPR

An important part of this thesis concerns structure determination by EPR, which is based upon the measurement of distances between pairs of spin labels. The measurement of distances makes use of the dipole-dipole interaction between the electron spins of two nitroxides. For nitroxide spin labels, the electron spin is considered to be localized in the center of the N-O bond. For systems where the distance between two spins is above 1 nm, the interaction of the spin can be described under the assumption of point-dipole approximation (86).

The dipole-dipole interaction (ν_{dd} in MHz units) between two spins is proportional to the inverse cube of the distance, and is given by (86)

$$\nu_{dd} = -\frac{\mu_0 \hbar}{8\pi^2}\frac{\gamma_A \gamma_B}{r_{AB}^3}(3\cos^2\theta - 1)$$

where μ_0 is the magnetic permeability at vacuum, γ_A and γ_B are the magnetogyric ratios for the two spins, $\hbar$ is the reduced Planck's constant, r_{AB} is the distance between the two spins, and θ is the angle between the spin-spin vector and the magnetic field.

The distance between pairs of spins can be measured by EPR in two ways depending on the distance; a) by cw-EPR and b) by a pulsed-EPR method called double electron-electron resonance (DEER), which is discussed below.

1.6.2.1 cw-EPR line broadening

Short distances up to 2 nm between two spins can be detected by cw-EPR. Figure 1.11 depicts the cw-EPR spectra of frozen nitroxides as a function of the dipolar interaction. The spectra are simulated using a dipolar tensor D, of the form

[- D - D + 2D] in which + 2D represents the parallel component of the dipolar tensor (D_{II}). Figure 1.11 shows the effect of the dipolar coupling on the lineshape of cw-EPR spectra of nitroxides, where the parallel component of the dipolar tensor was aligned either with the g_{yy} and A_{yy} direction or the g_{zz} and A_{zz} direction of the g and A tensors of the two nitroxides, assuming that the g and the A tensors of the two nitroxides are collinear. The direction of the principal axes of the g-tensor is indicated with blue dotted lines in Figure 1.9.

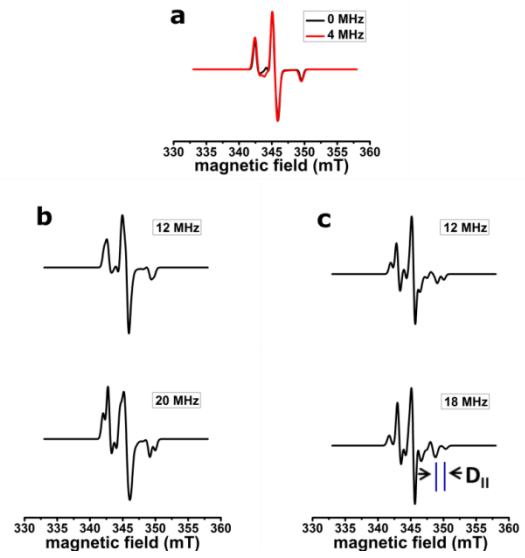

Figure 1.11. Effect of dipolar coupling on cw-EPR spectra of nitroxides at 120 K. a. Nitroxide spectrum simulated without dipolar interaction (black line) superimposed with simulated nitroxide spectrum for D = 4 MHz for D_{II} along the Z-direction (red line), b. simulated nitroxide spectrum showing dipolar line broadening and splitting at low and high field for D = 12 MHz (top) and D = 20 MHz (bottom) for D_{II} along the Y-direction, c. nitroxide spectrum showing dipolar line broadening and splitting at low field and high field for D = 12 MHz (top) and D = 18 MHz (bottom) for D_{II} along the Z-direction. The splitting of the line at high field marked by blue lines corresponds to 1.4 mT, i.e., 36 MHz (magnitude of D_{II} along the Z-direction). All the spectra were simulated with the algorithm "pepper" using the EasySpin (85) package. We used a g tensor [g_{xx} g_{yy} g_{zz}] = [2.009006 2.00687 2.003], and a hyperfine coupling [A_{xx} A_{yy} A_{zz}] = [13 13 100] MHz. The linewidth was kept fixed at 0.55 mT.

Figure 1.11a shows the superposition of the spectrum simulated for D = 0 MHz (Figure 1.11a, black line) with the spectrum for D = 4 MHz, and D_{II} along the Z-direction. This comparison depicts that the changes in lineshape become visible for dipolar coupling of D = 4 MHz (i.e., a distance of 2.35 nm between two spins). In Figure 1.11b, the parallel component was aligned with the Y-direction. For D = 12 MHz (i.e., a distance of 1.6 nm), the spectrum only slightly deviates from the one in the absence of dipolar interaction (Figure 1.11 b, top). With the increase of the D value to 20 MHz (i.e., a distance of 1.37 nm), a splitting of lines becomes visible (Figure 1.11 b, bottom). In Figure 1.11c, the D_{II} was aligned along the Z-direction. For D = 12 MHz (i.e., a distance of 1.6 nm), the splitting of the low-field and high-field lines becomes visible (Figure 1.11c, top). The splitting of the low-field and the high-field line becomes larger for D = 18 MHz (i.e., a distance of 1.4 nm) (Figure 1.11c, bottom). In this case, the splitting of the EPR line at high field (indicated with blue lines) corresponds to 36 MHz, i.e., the magnitude of D_{II}.

These simulations show how the lineshape varies with the orientation of the dipolar axis with respect to the g and A tensors of the nitroxides. The simulated effect is more pronounced than for real samples, which may be due to: a) in the simulation, D_{II} is aligned with a canonical orientation of the nitroxide, i.e., g_{yy} or g_{zz}, but arbitrary orientations of D_{II} will distribute the effect over the spectral lines, making the broadening less visible. b) the g-tensors of the two nitroxides are taken collinear in the simulation, while in practice this need not to be the case and there will be a distribution of orientations.

In chapter 6, we have used this method to derive inter-spin distances from line broadening in cw-EPR spectra.

1.6.2.2 Double electron-electron resonance (DEER)

For distances between two electron spins larger than 2 nm, their dipolar interaction becomes too weak to be detectable as a line broadening of transitions in cw-EPR spectra. Pulsed-EPR methods are available to determine the dipolar interaction in such cases and in our research we have made use of double electron-electron resonance (DEER) to access distances between 1.8 and 6 nm (87). The DEER pulse sequence is represented in Figure 1.12a. The two interacting spins are excited at distinct microwaves frequencies, the so-called observer and pump frequencies. The three-pulse excitation of one of the spins (the observer spin) results in a spin echo, as indicated in the top line. Excitation of the second spin, which is in interaction with the first one, with microwaves at the pump frequency and at a time between the second and third pulse at the observer frequency, results in a modulation of the echo intensity. The variation of the echo intensity as a function of the dipolar evolution time t is called the DEER-trace. As an example, Figure 1.12b, shows the DEER trace of a model sample, the biradical PH2, in which two nitroxide groups are covalently linked at a distance of 1.9 nm. The modulation at the frequency ν_{dd}, owing to the dipolar interaction between the two nitroxide spins, is clearly visible superimposed on the echo decay, which results from relaxation. For a distribution of distances between the two spins, for example for non-covalently bound nitroxide radicals, the modulation pattern will become less obvious or even smeared out completely, as illustrated in Figure 1.12c. In this case the separation of the effect of the dipolar interaction from other contributions to the echo decay becomes important. After subtraction of this background, the decrease of the echo intensity owing to the dipolar coupling remains and can be translated into a distribution of distances. The modulation

depth (λ) (Figure 1.12c) is related to the number of coupled spins that account for the measured DEER trace.

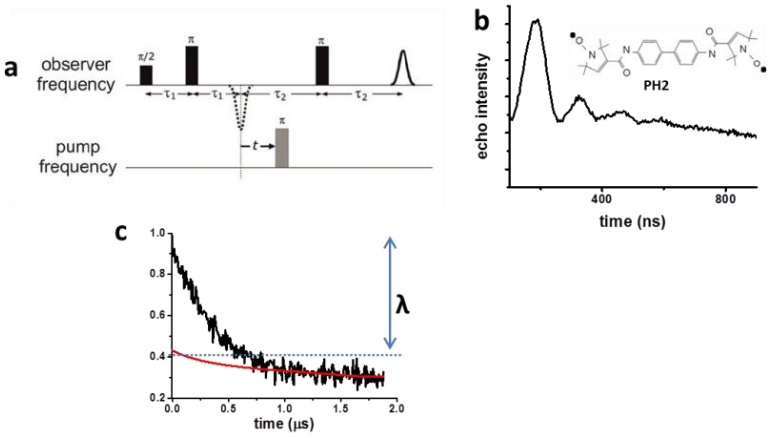

Figure 1.12. The DEER experiment. a. The DEER four-pulse sequence at two frequencies, the observer and the pump frequency. Delay times τ_1 and τ_2 are kept fixed, while the delay time t between the unobserved first echo (dotted line) and the pump pulse is varied. b. The measured DEER trace of a reference sample PH2 contains modulations, the period of which is related to the dipolar coupling between two electron spins. c. the DEER trace of a fibril sample (black line), which shows no modulations; the red line represents the background derived from the singly labelled proteins. The modulation depth (λ) represents the number of spins that contribute to the measured DEER trace.

For broad distance distributions, special attention has to be paid to the background, which is due to all interactions of spins that belong to all spin-labelled proteins, referred to as nano-objects (87,88). For a random distribution of these nano-objects, analytical background functions were calculated in (87,88). For soluble proteins, in buffer, the background is defined by a homogeneous 3D-background function, which describes the three-dimensional, random distribution of nano-objects in the sample (87–90). Such a background has been applied in chapter 6. The DEER traces of peptides or proteins bound to membranes can be corrected by a 2D background function, since membrane-bound proteins are randomly distributed in the plane of the lipid-bilayer(88,91). In

chapter 2 of this thesis, we derived the background function for the membrane-bound doubly-labelled proteins from that of the membrane-bound singly-labelled proteins. For the fibrils investigated in chapter 5, we encounter a special situation. For fibrils, the background dimensionality is expected to be close to a 1D-background function since the nano-objects, i.e., the doubly spin-labelled proteins are arranged preferentially in one dimension, which is along the fibril axis (Figure 1.6b, black arrow). Usually, the background function for fibrils is derived from the singly labelled proteins (chapter 5).

1.7 Thesis outline

In chapter 2, continuous wave (cw)-EPR is employed to investigate the interaction of αS with natural membranes. The membrane is presented in the form of SUVs, composed of lipids that mimic the natural membranes IMM and NPM. In the same chapter we examine the arrangement of αS on the membrane by measuring the distance between two spins on the same αS protein by double electron-electron resonance (DEER).

In chapter 3, we investigate the influence of phosphorylation on the binding of αS with model membranes by cw-EPR. We mimic the phosphorylation of αS at positon S87 and S129.

In chapter 4, the fibril morphology of αS is characterized by negative stain transmission electron microscopy (TEM). This study provides the necessary information about the fibril morphology.

In chapter 5, we investigate the fibril fold of αS by DEER. In this study we use the fibrils whose characterization was described in chapter 4.

In chapter 6, the arrangement of K/E peptides in their coiled-coil structure is investigated by cw-EPR and DEER, which reveals the orientation of the individual peptide in the coiled-coil structure.

1.8 References

1. Parkinson J. An Essay on the Shaking Palsy (Whitingham and Rowland, London). 1817.

2. Ozansoy M, Başak AN. The central theme of parkinson's disease: α-Synuclein. Mol Neurobiol. 2013;47:460–465.

3. De Rijk MC, Breteler MM, Graveland GA, Ott A, Grobbee DE, van der Meché FG, Hofman A. Prevalence of Parkinson's disease in the elderly: the Rotterdam Study. Neurology. 1995;45:2143–2146.

4. Cookson MR. α-Synuclein and neuronal cell death. Mol Neurodegener. 2009;4:9.
5. Gasser T. Molecular pathogenesis of Parkinson disease: insights from genetic studies. Expert Rev Mol Med. 2009;11:1-20.

6. Wolters EC. Non-motor extranigral signs and symptoms in Parkinson's disease. Parkinsonism Relat Disord. 2009;15:S6–S12.

7. Gasser T, Hardy J, Mizuno Y. Milestones in PD genetics. Mov Disord. 2011;26:1042–1048.
8. Dickson DW, Fujishiro H, Orr C, DelleDonne A, Josephs KA, Frigerio R, Burnett M, Parisi JE, klos KJ, Ahlskog JE. Neuropathology of non-motor features of Parkinson disease. Parkinsonism Relat Disord. 2009;15:S1–S5.

9. Spillantini M, Schmidt M, Lee V, Trojanowski J, Jakes R, Goedert M. α-Synuclein in Lewy bodies. Nature. 1997;388:839–840.

10. Spillantini MG, Crowther RA, Jakes R, Hasegawa M, Goedert M. α-Synuclein in filamentous inclusions of Lewy bodies from Parkinson's disease and dementia with Lewy bodies. Proc Natl Acad Sci U S A. 1998;95:6469–6473.

11. Maroteaux L, Campanelli JT, Scheller RH. Synuclein: a neuron-specific protein localized to the nucleus and presynaptic nerve terminal. J Neurosci. 1988;8:2804–2815.

12. Shumin Liu, Ipe Ninan, Irina Antonova, Fortunato Battaglia, Fabrizio Trinchese, Archana Narasanna, Nikolai Kolodilov, William Dauer, Robert D Hawkins OA. α-Synuclein produces a long-lasting increase in neurotransmitter release. EMBO J. 2004;23:4506–4516.

13. Uversky VN. Protein folding revisited. A polypeptide chain at the folding-misfolding-nonfolding cross-roads: which way to go? Cell Mol Life Sci. 2003;60:1852–1871.

14. Davidson WS, Jonas A, Clayton DF, George JM. Stabilization of α-Synuclein secondary structure upon binding to synthetic membranes. J Biol Chem. 1998;273:9443–9449.

15. Dunker AK, Lawson JD, Brown CJ, Williams RM, Romero P, Oh JS, Oldfield CJ, Campen AM, Ratliff CM, Hipps KW, Ausio J, Nissen MS, Reeves R, Kang C, Kissinger CR, Bailey RW, Griswold MD, Chiu W, Garner EC, Obradovic Z. Intrinsically disordered protein. J Mol Graph Model. 2001;19:26–59.

16. Dyson HJ, Wright PE. Intrinsically unstructured proteins and their functions. Nat Rev Mol Cell Biol. 2005;6:197–208.

17. Goedert M. The awakening of α-Synuclein. Nature. 1997;388:232–232.

18. Eliezer D, Kutluay E, Bussell R, Browne G. Conformational properties of α-Synuclein in its free and lipid-associated states. J Mol Biol. 2001;307:1061–1073.

19. Perrin RJ, Woods WS, Clayton DF, George JM. Interaction of human α-Synuclein and Parkinson's disease variants with phospholipids. Structural analysis using site-directed mutagenesis. J Biol Chem. 2000;275:34393–34398.

20. Jo E, McLaurin J, Yip CM, St. George-Hyslop P, Fraser PE. α-Synuclein membrane interactions and lipid specificity. J Biol Chem. 2000;275:34328–34334.

21. Jo E, Fuller N, Rand RP, St George-Hyslop P, Fraser PE. Defective membrane interactions of familial Parkinson's disease mutant A30P α-Synuclein. J Mol Biol. 2002;315:799–807.

22. Krüger R, Kuhn W, Müller T, Woitalla D, Graeber M, Kösel S, Przuntek H, Epplen JT, Schols L, Riess O. AlaSOPro mutation in the gene encoding α-Synuclein in Parkinson's disease. Nat Genet. 1998;18:106–108.

23. Zarranz JJ, Alegre J, Gómez-Esteban JC, Lezcano E, Ros R, Ampuero I, Vidal L, Hoenicka J, Rodriguez O, Atarés B, Llorens V, Gomez Tortosa E, del Ser T, Muñoz DG, de Yebenes JG. The new mutation, E46K, of α-Synuclein causes Parkinson and Lewy body dementia. Ann Neurol. 2004;55:164–173.

24. Polymeropoulos MH. Mutation in the α-Synuclein gene identified in families with Parkinson's disease. Science. 1997;276:2045–2047.

25. Lesage S, Anheim M, Letournel F, Bousset L, Honoré A, Rozas N, Pieri L, Madiona K, Dürr A, Melki R, Verny C, Brice A. G51D α-Synuclein mutation causes a novel Parkinsonian-pyramidal syndrome. Ann Neurol. 2013;73:459–471.

26. Appel-Cresswell S, Vilarino-Guell C, Encarnacion M, Sherman H, Yu I, Shah B, Weir D, Thompson C, Szu-Tu C, Trinh J, Aasly JO, Rajput A, Rajput AH, Jon Stoessl A, Farrer MJ. α-Synuclein p.H50Q, a novel pathogenic mutation for Parkinson's disease. Mov Disord. 2014;28:811–813.

27. Miake H. Biochemical characterization of the core structure of α-Synuclein filaments. J Biol Chem. 2002;277:19213–19219.

8. Fujiwara H, Hasegawa M, Dohmae N, Kawashima A, Masliah E, Goldberg MS, Shen J, Takio K, Iwatsubo T. α-Synuclein is phosphorylated in synucleinopathy lesions. Nat Cell Biol. 2002;4:160–164.

29. Takahashi M, Kanuka H, Fujiwara H, Koyama A, Hasegawa M, Miura M, Iwatsubo T. Phosphorylation of α-Synuclein characteristic of synucleinopathy lesions is recapitulated in α-Synuclein transgenic Drosophila. Neurosci Lett. 2003;336:155–158.

30. Okochi M, Walter J, Koyama a, Nakajo S, Baba M, Iwatsubo T, Meijer L, Kahle PJ, Haass C. Constitutive phosphorylation of the Parkinson's disease associated α-Synuclein. J Biol Chem. 2000;275:390–397.

31. Shimura H, Schlossmacher M, Hattori, N.Frosch M, Trockenbacher A, Schneider R, Mizuno Y, Kosik KS, Selkoe DJ. Ubiquitination of a new form of α-Synuclein by parkin from human brain: implications for Parkinson's disease. Science. 2001;293:263–269.

32. Hodara R, Norris EH, Giasson BI, Mishizen-Eberz AJ, Lynch DR, Lee VM, Ischiropoulos H. Functional consequences of α-Synuclein tyrosine nitration: diminished binding to lipid vesicles and increased fibril formation. J Biol Chem. 2004;279:47746–47753.

33. Crowther RA, Jakes R, Spillantini MG, Goedert M. Synthetic filaments assembled from C-terminally truncated α-Synuclein. FEBS Lett. 1998;436:309–312.

34. Braithwaite SP, Stock JB, Mouradian MM. α-Synuclein phosphorylation as a therapeutic target in Parkinson's disease. Rev Neurosci. 2012;23:191–198.

35. McFarland MA, Ellis CE, Markey SP, Nussbaum RL. Proteomics analysis identifies phosphorylation-dependent α-Synuclein protein interactions. Mol Cell Proteomics. 2008;7:2123–2137.

36. Clayton DF, George JM. The synucleins: a family of proteins involved in synaptic function, plasticity, neurodeneration and disease. Trends Neurosci. 1998;21:249–

254.

37. Burré J, Sharma M, Tsetsenis T, Buchman V, Etherton MR, Südhof TC. α -Synuclein promotes SNARE-complex assembly in vivo and in vitro. Science. 2010;329:1663–1667.

38. Nemani VM, Lu W, Berge V, Nakamura K, Onoa B, Lee MK, Chaudhry FA, Nicoll RA, Edwards RH. Increased expression of α-Synuclein reduces neurotransmitter release by inhibiting synaptic vesicle reclustering after endocytosis. Neuron. 2010;65:66–79.

39. Vila M, Ramonet D, Perier C. Mitochondrial alterations in Parkinson's disease: new clues. J Neurochem. 2008;107:317–328.

40. Devi L, Raghavendran V, Prabhu BM, Avadhani NG, Anandatheerthavarada HK. Mitochondrial import and accumulation of α-Synuclein impair complex I in human dopaminergic neuronal cultures and Parkinson disease brain. J Biol Chem. 2008;283: 9089–9100.

41. Devi L, Anandatheerthavarada HK. Mitochondrial trafficking of APP and α-Synuclein: Relevance to mitochondrial dysfunction in Alzheimer's and Parkinson's diseases. Biochim Biophys Acta. 2010;1802:11–19.

42. Li J, Uversky VN, Fink AL. Effect of familial Parkinson's disease point mutations A30P and A53T on the structural properties, aggregation, and fibrillation of human α-Synuclein. Biochemistry. 2001;40:11604–11613.

43. Ulmer TS, Bax A. structure and dynamics of micelle-bound human α-Synuclein. J Biol Chem. 2005;280:9595–9603.

44. Ulmer TS, Bax A. Comparison of structure and dynamics of micelle-bound human α-Synuclein and Parkinson disease variants. J Biol Chem. 2005;280:43179–43187.

45. Georgieva ER, Ramlall TF, Borbat PP, Freed JH, Eliezer D. The lipid-binding domain of wild type and mutant α-Synuclein: compactness and interconversion between the broken and extended helix forms. J Biol Chem. 2010;285:28261–28274.

46. Georgieva ER, Ramlall TF, Borbat PP, Freed JH, Eliezer D. Membrane-bound α-Synuclein forms an extended helix: long-distance pulsed ESR measurements using vesicles, bicelles, and rodlike micelles. J Am Chem Soc. 2008;130:12856–12857.

47. Eliezer D, Kutluay E, Bussell R, Browne G. Conformational properties of α-Synuclein in its free and lipid-associated states. J Mol Biol. 2001;307:1061–1073.

48. Dikiy I, Eliezer D. Folding and misfolding of α-Synuclein on membranes. Biochim Biophys Acta - Biomembr. 2012;1818:1013–1018.

49. Haque F, Pandey AP, Cambrea LR, Rochet J-C, Hovis JS. Adsorption of α-Synuclein on lipid bilayers: modulating the structure and stability of protein assemblies. J Phys Chem B. 2010;114:4070–4081.

50. Drescher M, Van Rooijen BD, Veldhuis G, Subramaniam V, Huber M. A sTable lipid-induced aggregate of α-Synuclein. J Am Chem Soc. 2010;132:4080–4082.

51. Bekshe Lokappa S, Ulmer TS. α-Synuclein populates both elongated and broken helix states on small unilamellar vesicles. J Biol Chem. 2011;286:21450–21457.

52. Drescher M, Veldhuis G, Van Rooijen BD, Milikisyants S, Subramaniam V, Huber M. Antiparallel arrangement of the helices of vesicle-bound α-Synuclein. J Am Chem Soc. 2008;130:7796–7797.

53. Fusco G, De Simone A, Gopinath T, Vostrikov V, Vendruscolo M, Dobson CM, Veglia G. Direct observation of the three regions in α-Synuclein that determine its membrane-bound behaviour. Nat Commun. 2014;5:1-8.

54. Middleton ER, Rhoades E. Effects of curvature and composition on α-Synuclein binding to lipid vesicles. Biophys J. 2010;99:2279–2288.

55. Rhoades E, Ramlall TF, Webb WW, Eliezer D. Quantification of α-Synuclein binding to lipid vesicles using fluorescence correlation spectroscopy. Biophys J. 2006;90:4692–4700.

56. Drescher M, Godschalk F, Veldhuis G, van Rooijen BD, Subramaniam V, Huber M. Spin-label EPR on α-Synuclein reveals differences in the membrane binding affinity of the two antiparallel helices. ChemBioChem. 2008;9:2411–2416.

57. Jao CC, Hegde BG, Chen J, Haworth IS, Langen R. Structure of membrane-bound α-Synuclein from site-directed spin labeling and computational refinement. Proc Natl Acad Sci U S A. 2008;105:19666–19671.

58. Robotta M, Braun P, van Rooijen B, Subramaniam V, Huber M, Drescher M. Direct evidence of coexisting horseshoe and extended helix conformations of membrane-bound α-Synuclein. ChemPhysChem. 2011;12:267–269.

59. Kumar P, Segers-Nolten IMJ, Schilderink N, Subramaniam V, Huber M. Parkinson's protein α-Synuclein binds efficiently and with a novel conformation to two natural membrane mimics. PLoS One. 2015;10:1-11.

60. Robotta M, Hintze C, Schildknecht S, Zijlstra N, Jüngst C, Karreman C, Huber M, Leist M, Subramaniam V, Drescher M. Locally resolved membrane binding affinity of the N-terminus of α-Synuclein. Biochemistry. 2012;51:3960–3962.

61. Robotta M, Gerding HR, Vogel A, Hauser K, Schildknecht S, Karreman C, Leist M, Subramaniam V, Drescher M. Alpha-Synuclein binds to the inner membrane of mitochondria in an α-helical conformation. Chembiochem. 2014;1–4.

62. Högen T, Levin J, Schmidt F, Caruana M, Vassallo N, Kretzschmar H, Botzel K, Kamp F, Giese A. Two different binding modes of α-Synuclein to lipid vesicles depending on its aggregation state. Biophys J. 2012;102:1646–1655.

63. Jao CC, Der-Sarkissian A, Chen J, Langen R. Structure of membrane-bound α-Synuclein studied by site-directed spin labeling. Proc Natl Acad Sci U S A. 2004;101:8331–8336.

64. Bortolus M, Tombolato F, Tessari I, Bisaglia M, Mammi S, Bubacco L, Ferrarini A, Maniero AL. Broken helix in vesicle and micelle-bound α-Synuclein: insight from site-directed spin labelling-EPR experiments and MD simulations. J Am Chem Soc. 2008;130:6690–6691.

65. Anderson JP, Walker DE, Goldstein JM, De Laat R, Banducci K, Caccavello RJ, Barbour R, Huang J, Kling K, Lee M, Diep L, Keim PS, Shen X, Chataway T, Schlossmacher MG, Seubert P, Schenk D, Sinha S, Gai WP, Chilcote TJ. Phosphorylation of Ser-129 is the dominant pathological modification of α-Synuclein in familial and sporadic Lewy body disease. J Biol Chem. 2006;281:29739–29752.

66. Sato H, Kato T, Arawaka S. The role of Ser129 phosphorylation of α-Synuclein in neurodegeneration of Parkinson's disease: a review of in vivo models. Rev Neurosci. 2013;24:115–123.

67. Paleologou KE, Oueslati A, Shakked G, Rospigliosi CC, Kim H-Y, Lamberto GR, Fernandez CO, Schmid A, Chegini F, Gai WP, Chiappe D, Moniatte M, Schneider BL, Aebischer P, Eliezer D, Zweckstetter M, Masliah E, Lashuel HA. Phosphorylation at S87 Is enhanced in synucleinopathies, inhibits α-Synuclein oligomerization, and influences Synuclein-membrane interactions. J Neurosci. 2010;30:3184–3198.

68. Goedert M. α-Synuclein and neurodegenerative diseases. Nat Rev Neurosci. 2001;2:492–501.

69. Crowther RA, Daniel SE, Goedert M. Characterisation of isolated α-Synuclein filaments from substantia nigra of Parkinson's disease brain. Neurosci Lett. 2000;292:128–130.

70. Fändrich M. On the structural definition of amyloid fibrils and other polypeptide aggregates. Cell Mol Life Sci. 2007;64:2066–2078.

71. Jimenez JL, Nettleton EJ, Bouchard M, Robinson C V, Dobson CM, Saibil HR. The protofilament structure of insulin amyloid fibrils. Proc Natl Acad Sci U S A. 2002;99:9196–9201.

72. Fändrich M, Meinhardt J, Grigorieff N. Structural polymorphism of Alzheimer Abeta and other amyloid fibrils. Prion. 2009;3:89–93.

73. Meinhardt J, Sachse C, Hortschansky P, Grigorieff N, Fändrich M. Aβ(1-40) fibril polymorphism implies diverse interaction patterns in amyloid fibrils. J Mol Biol. 2009;386:869–877.

74. Petkova AT, Leapman RD, Guo Z. Self-propagating ,molecular-level polymorphism in Alzheimer ’s Aβ-amyloid fibrils. 2005;307:262–265.

75. Heise H, Hoyer W, Becker S, Andronesi OC, Riedel D, Baldus M. Molecular-level secondary structure, polymorphism, and dynamics of full-length α-Synuclein fibrils studied by solid-state NMR. Proc Natl Acad Sci U S A. 2005;102:15871-15876.

76. Weber T, Zemelman BV., McNew JA, Westermann B, Gmachl M, Parlati F, Sollner TH, Rothman JE. SNAREpins: Minimal Machinery for Membrane Fusion. Cell. 1998;92:759–772.

77. van den Bogaart G, Jahn R. Insight to membrane fusion. Proc Natl Acad Sci U S A. 2011;108:11729–11730.

78. Hashemi Shabestari M. Spin-label EPR on disordered and amyloid proteins. Thesis, Leiden University Repository. 2013.

79. Sutton RB, Fasshauer D, Jahn R, Brunger AT. Crystal structure of a SNARE complex involved in synaptic exocytosis at 2.4 Å resolution. Nature. 1998;395:347–353.

80. Jahn R, Lang T, Südhof TC. Membrane Fusion. Cell. 2003;112:519–533.

81. Litowski JR, Hodges RS. Designing heterodimeric two-stranded α-helical coiled-coils. Effect of hydrophobicity and alpha-helical propensity on protein folding, stability, and specificity. J Biol Chem. 2002;277:37272–37279.

82. Hubbell WL, Altenbach C. Investigation of structure and dynamics in membrane proteins using site-directed spin labeling. Curr Opin Struct Biol. 1994;4:566–573.

83. Hubbell WL, Mchaourab HS, Altenbach C, Lietzow MA. Watching proteins move using site-directed spin labeling. Structure. 1996;4:779–783.

84. Hubbell WL, Cafiso DS, Altenbach C. Identifying conformational changes with site-directed spin labeling. Nat Struct Biol. 2000;7:735–739.

85. Stoll S, Schweiger A. EasySpin, a comprehensive software package for spectral simulation and analysis in EPR. J Magn Reson. 2006;178:42–55.

86. Jeschke G. Determination of the Nanostructure of Polymer Materials by Electron Paramagnetic Resonance Spectroscopy. Macromol Rapid Commun. 2002;23:227–246.

87. Jeschke G. Distance measurements in the nanometer range by pulse EPR. ChemPhysChem. 2002;3:927–932.

88. Jeschke G, Chechik V, Ionita P, Godt A, Zimmermann H, Banham J, Timmel CR, Hilger D, Jung H. DeerAnalysis2006 - a comprehensive software package for analyzing pulsed ELDOR data. Appl Magn Reson. 2006;30:473–498.

89. Steigmiller S, Börsch M, Gräber P, Huber M. Distances between the b-subunits in the tether domain of F0F1-ATP synthase from E. coli. Biochim Biophys Acta - Bioenerg. 2005;1708:143–153.

90. Jeschke G, Koch A, Jonas U, Godt A. Direct conversion of EPR dipolar time evolution data to distance distributions. J Magn Reson. 2002;155:72–82.

91. Hilger D, Jung H, Padan E, Wegener C, Vogel KP, Steinhoff HJ, Jeschke G. Assessing oligomerization of membrane proteins by four-pulse DEER: pH-dependent dimerization of NhaA Na+/H+ antiporter of E. coli. Biophys J. 2005;89:1328–1338.

92. Pasanen P, Myllykangas L, Siitonen M, Raunio A, Kaakkola S, Lyytinen J, Tienari PJ, Pöyhönen M, Paetau A. Novel α-Synuclein mutation A53E associated with atypical multiple system atrophy and Parkinson's disease-type pathology. Neurobiol. Aging. 2014;35:2180.e1-2180.e5.